Thermal transport properties in amorphous/nanocrystalline metallic composites: A microscopic insight

Amani Tlili, S. Pailhes, R. Debord, Beatrice Ruta, J. -J. Gravier, J.J Blandin, Nicholas Blanchard, S. Gomes, A. Assy, A. Tanguy, et al.

Thermal transport properties in amorphous/nanocrystalline metallic composites: a microscopic insight

A. Tlili[a,b],V. M. Giordano[a 1], R. Debord[a],B. Ruta[a,c],S. Gravier[b,d],J.-J. Blandin[b,d],N. Blanchard[a],S. Gomès[e],A. Assy[e],A. Tanguy[f],S. Pailhès[a]

a Institute of Light and Matter, UMR5306 Université Lyon 1-CNRS, Université de Lyon 69622 Villeurbanne cedex, France

b Université Grenoble Alpes, SIMAP, F-38000 Grenoble, France

c ESRF-The European Synchrotron, CS 40220, 38043 Grenoble Cedex 9, France

d CNRS, SIMAP, F-38000 Grenoble, France

e Université de Lyon, CNRS, CETHIL UMR5008, F-69621 Villeurbanne, France

f Université de Lyon, LaMCoS, INSA-Lyon, CNRS UMR5259, F-69621, France

Abstract

In the last years new composite materials made of a metallic glass matrix with embedded nanocrystals have arisen as a promising alternative to the metallic glasses, due to their higher hardness. Although the effects of a partial nanocrystallization onto mechanical and magnetic properties have been widely investigated, nothing is known about thermal transport properties, interesting for recently proposed novel applications. Here we investigate how thermal transport is modified in presence of nanocrystalline inclusions in a Zr-based bulk metallic glass. By means of electric measurements and inelastic x ray scattering we are able to disentangle the effects of a partial nanocrystallization onto the two different contributions to heat transport, the electronic and the vibrational one. We show that no enhanced electrons or phonons scattering from the interfaces is observed, while the presence of crystalline nanoinclusions leads to an increase of both contributions, via an increased electric conductivity and transverse acoustic speed of sound. Surprisingly, while a gradual modification of the electric

[1]Corresponding Author: valentina.giordano@univ-lyon1.fr

conductivity with the crystalline fraction is observed, even a low crystalline fraction is sufficient to modify elastic and vibrational properties. Our results indicate that low crystallinity composites are indeed promising alternative to both amorphous and crystalline alloys, thanks to their unique combination of high ductility, polycrystal-like vibrational properties and amorphous-like electric transport.

Keywords: `Transport properties,Bulk metallic glasses, Composites, phonons`

---

1. Introduction

In the last decades, Metallic Glasses (MG) have aroused as revolutionary materials in a number of structural applications, due to their excellent mechanical properties, intimately related to their disordered atomic structure [1, 2, 3]. Despite their great potential, however, their widespread use has long been hindered by their inherent brittleness, displayed under plastic deformation below the glass transition temperature, and related to shear bands instability [1, 4]. Several ways have been explored to overcome the MG macroscopic brittlelike behavior, among which material size reduction, for playing on the surface to volume ratio to increase the ductility, chemical composition tuning, for playing on the kind of atomic bonding, or partial nanocrystallization. This latter appears as a simple and most promising way, as it can be realized very easily, by means of a variety of procedures, from compression to nanoindentation to controlled thermal protocols [5, 6].

Whatever the method, a microstructure with a variable density of nanometer-sized crystalline particles embedded in an amorphous matrix is obtained, which has been found to display a higher hardness and in some cases an improved ductility with respect to the parent glassy phase, both under compression and tensile strength [7, 8, 9, 10, 11]. Such improvement has been understood in terms of an active role of the precipitates in changing the shear bands propagation, thus confining the deformation [12]. Starting from this, partially crystallized

MG have been the subject of intense studies, with the aim of identifying the conditions for which the functional properties are not lessened by the partial crystallization while the mechanical resistance is increased.

At this day, investigations have mainly focused on the effect of nanocrystallites on mechanical [13, 14, 15] and magnetic [16, 17] properties. However, a more global understanding of their influence on all different properties is needed for allowing to expand the application fields of metallic glasses composites. Indeed, many novel applications have been recently proposed for MG, exploiting the combination of their excellent mechanical properties with other functional properties, such as thermal and electronic transport. A recent example is the investigation of the potential of MG as alternative thermal barrier coating materials (TBC), on substrates where classical ceramic coatings are not appropriate [18, 19, 20], which takes advantage of their unusual combination of a relatively low thermal conductivity with a metallic electric character, together with a reduced thermal expansion.

So far, only data on thermal conductivity of fully amorphous [21, 22] or crystalline phases [22] have been reported, the information on a partial nanocrystallization effect is dramatically lacking. Still, some insight could be obtained from the electric transport properties, as in metallic systems electrons are the dominating heat carriers and their contribution to the thermal conductivity is proportional to the electric one.

It is largely known that electrical resistivity decreases upon crystallization [23, 24, 25], reaching values typical for a metallic polycrystal, and it has been observed that such a decrease can be accompanied by a change in the temperature behavior: in the polycrystal, the resistivity increases with temperature, as typically for metals [26], while in glasses the behavior depends on the specific alloy composition [27, 28]. During crystallization, the resistivity decrease is generally assumed to be linear with the crystalline fraction, and, as such, it has often been used to monitor crystallization [29, 30, 31, 32]. However, a non monotonic evolution has been reported in a $Cu_{46}Zr_{46}Al_8$ MG [33], with an increase in the early

stages of crystallization, followed by the usual decrease. Such behavior has been explained in terms of a strong electron scattering at the amorphous/crystalline interfaces, due to the precipitation of a high density of very small ($\approx 1-2$ nm) nanocrystals at the beginning, which decreases with the proceeding of crystallization when nuclei start to grow.

To our knowledge, nothing exists yet in the literature on how the vibrational contribution to the thermal conductivity can be affected by the nanocrystalline inclusions. For understanding it, a microscopic investigation of the properties of the quasi-particles responsible for this contribution, the phonons, is required.

Here we tackle this problem, using a combined macroscopic/microscopic approach to disentangle the effect of a partial nanocrystallization on the electronic and vibrational contributions to heat transport in a Zr-based MG, chosen because of its good combination of strength, ductility, corrosion resistance and large glass forming ability, which make it suitable for massive industrial production and applicability.
We find that the electronic contribution to the thermal conductivity gradually and weakly increases with the crystalline fraction, as can be predicted using an effective medium theory, where interfaces don't play any major role in the range of crystalline fractions investigated. No interface-related enhanced phonons scattering can be detected neither on the vibrational contribution, the partial nanocrystallization causing only a slight increase of the transverse sound velocity, and thus of the macroscopic shear modulus, towards the crystalline value. The global effect is an increased total thermal conductivity, mostly due to the electronic contribution.

The paper is structured as follows: in section 2, we give details on the experimental methods used for this investigation, then in section 3 we report on sample preparation and focus on the different contributions to the thermal conductivity: the electric one (section 3.3) and the vibrational one (section 3.4).

All results are thus globally discussed in the last section.

2. Experimental Methods

$Zr_{52.5}Cu_{27}Al_{10}Ni_8Ti_{2.5}$ metallic glass rods (3 mm diameter, 8 cm length) were prepared by arc-melting the pure elements in stoichiometric concentration under argon atmosphere and quenching the master alloy in a water-cooled copper mold. The fully amorphous character of the alloy was confirmed by x-ray diffraction (XRD) at T=300K prior to any processing. Discs 300 μm to 2 mm thick were then cut from the rod for further analysis and amorphous/crystalline composites preparation.

The crystallization process was monitored by differential scanning calorimetry (DSC) using the Diamond apparatus from Perkin Elmer. Structural characterization, aiming to confirm the predicted crystalline fraction, and measure the crystalline grains size distribution was done by means of XRD and transmission electron microscopy (TEM). XRD was performed at the X-ray diffraction center Henry Lonchambon, Lyon, using a D8 Advanced diffractometer in Bragg-Brentano geometry with $\lambda = 1.541\mathring{A}$, while TEM was performed using a JEOL JEM2100 equipped with a LaB6 thermionic electron gun and a High Tilt objective pole piece. The microscope was operated at 200 keV with a point-to-point resolution of 0.25 nm. The samples were mounted on a double-tilt beryllium sample holder and the images were recorded on a Gatan Orius SC1000 bottom mount CCD camera, 4008 x 2672 pixels with a physical size of 9μm each. For TEM measurements, samples were prepared by using a precision ion polishing system (PIPS, Gatan 691 model) in top-bottom mode at 2.5kV with a milling angle of $\pm 4^\circ$, the instrumental parameters having been chosen in order to hinder any ion beam induced crystallization [34, 35, 12].

Electric transport measurements were performed by means of the Van Der Pauw technique using a home-made apparatus working between 50 and 300 K. Room temperature absolute values were counter-checked using a commercial 4 points probe. Thermal conductivity was measured by means of the Thermal Scanning

Microscopy technique (SThM) at the Cethil, in Lyon [36, 37], on samples polished with a 0.5 μm diamond powder.

In order to get insight into the vibrational contribution to thermal transport, phonon dispersions were measured by inelastic X-ray scattering (IXS) at the ID28 beamline of the ESRF, Grenoble. A high energy resolution of ≈ 2.8 meV was reached using the (9,9,9) reflection of the silicon crystal monochromator, corresponding to an incident x-ray energy of 17.794 keV (wavelength $\lambda_0 = 0.6968\mathring{A}$). The beam was focused into a spot of $150(H) \times 90(V)$ μm (FWHM) on the sample, which was hosted in a vacuum chamber for avoiding any small angle scattering from the air. Spectra were collected in a fixed-q scanning-energy mode at a given position of the analyser chamber, hosting 9 analysers at different scattering angles 2θ, thus allowing for simultaneously collecting 9 different momentum transfers $q = \frac{4\pi}{\lambda_0} sin(\theta)$. Details on the IXS setup can be found elsewhere [38, 39, 40].

3. Results and discussion

3.1. Samples preparation

Amorphous/crystalline composites were prepared by isothermally annealing the glass at a temperature lying between the glass transition and the crystallization temperature, monitoring the crystallization by DSC. In order to hinder the crystalline growth and get nanometric crystalline grains, the highest available heating ramp was used, 100 K/min, for which a glass transition (T_g) and crystallization (T_x) temperature of 719 K and 789.5 K have been respectively measured. On the basis of this information, we have chosen as target temperature for the partial crystallization protocol T_a=740 K and performed an isothermal DSC experiment to first characterize the whole crystallization process. This has allowed us to extract the annealing time dependence of the crystalline fraction from the calorimetric signal, as done in Ref. [[41]], and use it as a guide for preparing amorphous/nanocrystalline composites with different

crystalline fractions, by changing the annealing time at $T = T_a$, while following the calorimetric signal.

Fig. 1 reports some representative XRD spectra for samples with a crystalline fraction going from 0 to 100%. The position $q_0 = 26$ nm^{-1} of the First Sharp Diffraction Peak (FSDP) in the fully amorphous sample ($x = 0$) is marked by a vertical dashed line, and nicely correspond to the most intense peaks in the partially and totally crystalline samples. Crystallization is accompanied by the growing up of broad peaks, clearly associated to the presence of nanometric crystallites, being the broadening inversely proportional to the crystallite size.

It is possible to estimate the amorphous fraction (and thus the crystalline one) in the composite, by directly comparing the XRD pattern collected on the amorphous phase prior to crystallization and the one after the thermal protocol. The procedure is simplified by the fact that the two patterns were collected on the very same sample and in the same experimental conditions, which means that incident intensity and background signal were the same. As the number and chemical identity of atoms contributing to the signal remains the same, the ratio of the amorphous component in the composite pattern to the total amorphous signal reflects the volumetric amorphous fraction.
More specifically, after background subtraction, we superpose the amorphous and composite patterns, and we identify the scaling parameter for which the amorphous signal matches the composite one in the q regions between crystalline peaks, where the intensity comes mostly from the amorphous component (Fig. 1 right panel). Such scaling parameter gives the volumetric amorphous fraction in the composite within $\approx 5\%$.

Once the amorphous content is known, its signal can be subtracted from the composite pattern in order to get the purely crystalline signal and analyze the crystalline peaks. Contributions from three different crystalline phases can be identified, Zr_2Ni, Zr_2Cu and Zr_7Cu_{10}, the latter being the major one. From the

width of the diffraction peaks the crystallites size has been estimated by means of the Scherrer method [42] and found to be in the [5-20] nm range depending on the sample.

In order to confirm the results of our XRD analysis, the same samples, after having performed all the transport measurements, have been investigated by TEM. The samples have been first mechanically polished to decrease their thickness to less than 50 μm, and then a hole was drilled by PIPS. The hole borders, which have thicknesses less than 200 nm, were then imaged by high-resolution TEM, which allows to clearly distinguish the lattice planes in the crystalline zones, and thus identify the crystallites in the amorphous matrix. For each sample, several images were taken along the hole border, and analyzed in order to extract the total crystalline over amorphous areas, and the size distribution for the observed crystallites. An example of a TEM image is reported in Fig. 2, where we find a crystalline volume fraction of 50% and an average grain size of $d \approx 4 \pm 2$ nm, whose distribution is reported in the inset.
The results of the TEM investigations were found to be in good agreement with the XRD estimates, as well as with the predicted DSC crystalline fractions.

3.2. Thermal Transport

As first thing, the room temperature thermal conductivity of the metallic glass, a fully crystalline sample and a composite with 30% crystalline fraction has been measured by scanning thermal microscopy [36, 37]. No difference could be assessed within the experimental uncertainty, as large as 25%, due to the intrinsic uncertainty of the method and to the surface roughness. Indeed, we found a thermal conductivity of $k_T = 5$ $WK^{-1}m^{-1}$ in the glass and 4.6 and 4.7 in the composite and polycrystal respectively. Such a low value in the fully crystalline sample is surprising, and can be understood in terms of a heat transport dominated by grain boundaries scattering in the nanometric polycrystal, decreasing its thermal conductivity towards the amorphous value. The crystalline fraction-independence, on the other hand, suggests a negligible effect of

a partial nanocrystallization on the thermal transport, at least for a crystalline fraction of 30%.

As previously mentioned, the total thermal conductivity is the sum of two contributions, one coming from the electrons, k_{el}, and the other from the atomic vibrations, k_{at}. One could thus wonder whether a lucky compensation of opposite trends in the two contributions could lead to a crystallinity-independent thermal conductivity. In order to disentangle the interface and partial nanocrystallization effect on the two contributions, we have performed a separate detailed investigation of both.

3.3. Electronic transport

The electronic contribution is intimately linked to the electric conductivity, the Wiedemann-Franz law assessing their proportionality for simple systems: $k_{el} = \frac{LT}{\rho}$, with $L = 2.45 \times 10^{-8}$ W Ω K^{-2} the Lorenz number, T and ρ temperature and electrical resistivity respectively. While this law is not universally valid, the Lorenz number possibly being different and temperature dependent, its validity in metallic glasses has been confirmed in several cases [24, 43, 21, 44] with the given value for L.

We have thus investigated the electrical resistivity of amorphous/nanocrystalline composites between 50 and 300 K for getting insight into the electronic contribution. The observed temperature and crystalline fraction dependencies are reported in Fig. 3 (a) and (b).

As expected, the room temperature resistivity decreases with the crystalline fraction, but with a total decrease of only 20% from amorphous to fully crystalline sample. Such a small difference, contrasting with literature data on the devitrification of some MG leading to polycrystals with micrometric grains, can be ascribed to the nanocrystallinity of the fully crystallized sample, giving raise to a grain boundary dominated transport.

Looking at the temperature dependence, it can be seen that all samples but the fully crystalline one display a negative dependence, the resistivity decreas-

ing with temperature, as can be quantified via the Temperature Coefficient of Resistivity $TCR = \frac{\delta\rho(T)}{\delta T}\frac{1}{\rho_{50\,K}}$ reported in Fig. 3 (c). Such behavior in the glass is not the mark of a semiconducting nature of the system, but can be explained in terms of an important electron localization. Indeed, according to Mizutani's classification of metallic glasses [28, 27], our system belongs to the fourth group, which gathers glasses where the electric transport is dominated by the d-electrons, resulting in a relatively high room temperature electrical resistivity (between 100 and 200 $\mu\Omega$ cm). In such systems, the temperature behavior of this latter can be described by the Baym-Mesel-Cote theory [45], giving $\rho(T) = (\rho_0 + \alpha T)e^{-W}$, with ρ_0 the residual resistivity at T=0 K and W the Debye-Waller factor. A negative temperature dependence can here be expected for temperatures above ≈20 K, due to the main role played by the Debye-Waller factor [28, 27].

Inversely, the resistivity of the fully crystalline sample exhibits the normal metal-like temperature increase, with a linear dependence typical for polycrystalline materials with nanometric grains, due to the dominant interface effect [26]. From the negative TCR in all composites, we can thus conclude that electric transport is dominated by the matrix even for crystalline fractions as large as 50%.

The behaviors of $\rho(x)$ and the TCR are rather smooth, revealing no enhanced interface effect such as the one reported in Ref.[[33]], where interface scattering caused a maximum in the electrical resistivity at small crystalline fractions. The behaviors here look in fact quite linear, suggesting that a simple Effective Medium Theory (EMT) could capture the mechanisms at play. This is indeed the case: we can reproduce both crystalline fraction dependencies using the model developed in Ref. [[46]], which, in presence of two phases, leads to the following equality:

$$x\frac{\sigma_c(T) - \sigma_e(T)}{\sigma_c(T) + 2\sigma_e(T)} + (1-x)\frac{\sigma_a(T) - \sigma_e(T)}{\sigma_a(T) + 2\sigma_e(T)} = 0; \quad (1)$$

where x is the crystalline fraction, σ the electrical conductivity and subscripts

c, a and e stand for crystalline, amorphous and effective medium. For the two phases, we use the measured values of the temperature dependence of the electrical conductivity $\sigma(T) = 1/\rho(T)$ for the glass and the fully crystalline sample. This choice corresponds to the idea that the crystalline component being made of nanometric grains, its electrical conductivity is given by the one measured on a polycrystal with nanometric grains. In this sense σ_c implicitly includes the effect of the finite size on the electric transport of isolated nanometric grains. With this assumption, Eq. 1 gives a calculated electrical resistivity and TCR in a very good agreement with our measurements, as can be seen in Fig. 3 where they are reported as dashed lines. Moreover, the model allows us to estimate $x_c = 60\%$ as the critical value of crystallinity for which the crystalline part starts to dominate over the matrix, causing the change of sign in the TCR.

3.4. Phonons transport

The understanding of the partial nanocrystallization effect onto the second contribution to thermal conductivity requires a microscopic investigation: we are here interested to heat transported by collective atomic vibrations, described by quasi-particles called phonons, characterized by a wavevector q (or wavelength $\lambda = 2\pi/q$), an energy $E = \hbar\omega$ and a lifetime τ (or phonon broadening $\Gamma = 1/\tau$). In its lifetime, a phonon with velocity $v = \hbar\omega/q$ transports over its mean free path $l = v\tau$ a quantum of heat equal to its velocity times its energy. It follows that the total vibrational contribution can be expressed as an integral over all phonon frequencies [47, 48]:

$$k_{at} = 1/3 \int C_v(\omega) v(\omega) l(\omega) \tau(\omega) g(\omega) d\omega; \tag{2}$$

with $C_v(\omega)$ and $g(\omega)$ the phonon specific heat and density of states.
Such formulation, developed in the framework of the relaxation time approximation of the Boltzmann transport theory in crystalline systems, can still be used in amorphous systems, as it has been derived by Allen and Feldman [49, 50], provided that the calculation is limited to low energy phonons, which are not over-

damped and can still be considered as propagative modes. When the phonon mean free path becomes comparable with the phonon wavelength, $l \approx \lambda/2$ (Ioffe-Regel limit), the phonon stops to be propagative and thermal transport becomes diffusive.

The vibrational thermal conductivity cannot be experimentally directly accessed, unless the system is insulator so that the total thermal conductivity coincides with the vibrational one. However it is possible to measure the phonon individual properties in a given energy range by means of inelastic scattering techniques, and estimate the right side of Eq. 2.

We have thus performed an inelastic X ray experiment collecting data on three samples: an amorphous, a fully crystalline and a partially crystallized one with x=30%. A total of 27 q-points was measured per sample up to the maximum of the static structure factor, $q_0 = 26$ nm^{-1}.

It is now largely accepted that in a disordered system a pseudo-Brillouin zone can be identified with $q_0/2$ marking its border. Concerning the polycrystalline sample, the first strong diffraction peak allows similarly to identify an orientationally averaged pseudo-Brillouin zone, which is pertinent for the comparison with the amorphous dynamics data [51]. A selection of spectra of the three samples is reported in Fig. 4, for positive energy transfer, and after subtraction of the elastic line. As it can be seen, the inelastic excitation remains well defined, although broad, up to very high momentum transfer.

Data have been analyzed using a Damped Harmonic Oscillator (DHO) model for the inelastic excitation and a delta function for the elastic line, convoluted with the experimental resolution [52].

In all samples, two inelastic excitations were needed to fit data for $q \geq 7$ nm^{-1}, while in the partially and fully crystalline samples up to three modes were needed in the second pseudo-Brillouin Zone ($q \geq q_0/2$). The highest energy mode was ascribed to a longitudinal excitation, while the lower ones to transverse-like excitations. Their respective phonon velocities and broadening are reported in Fig. 5 and 6.

The fact that we can easily identify only one longitudinal and one transverse mode in the first pseudo-Brillouin zone in the polycrystal is not trivial. It is known that in a polycrystal the measurement should yield the orientational average of phonons belonging to all existing branches with the same polarization, and the broadening corresponds to the width of the branches distribution [53, 51]. One single mode per polarization should thus be observed in the first pseudo-Brillouin zone for a single-phase polycrystal with randomly oriented grains. In presence of several phases, as it is the case here, more branches could be observed, one per crystalline phase and per polarization. The observation of only one longitudinal and one transverse mode in the first pseudo-Brillouin zone is thus an indication that phonon dynamics is dominated by the major crystalline phase.

3.4.1. Longitudinal Modes

Looking at the longitudinal speed of sound, the amorphous sample exhibits a positive dispersion, in the sense that the low-q limit of its sound velocity (as measured at high frequency here) is slightly higher than the macroscopic limit as measured by ultrasound techniques at low frequency. Discrepancies between high frequency and low frequency sound velocity have already been reported in a number of molecular [52] and metallic glasses [54, 55] and ascribed to the existence of nanometric elastic heterogeneities or relaxation processes [56].

No difference among the three samples is observed over the whole explored q-range, indicating that the longitudinal moduli of the three samples are very similar in the investigated lengthscale, which leads to the conclusion that they have similar local orders and similar inter-atomic forces.

Concerning the longitudinal phonon broadening, it increases in the first half of the pseudo-Brillouin Zone, before the appearance of the transverse acoustic excitation, then it starts to flatten out. While in the glass this is inversely proportional to phonon lifetime, this is not true in the polycrystal, where broadening is related to the branches separation. It is thus surprising that the broaden-

ing in the polycrystal is only slightly smaller than in the glass, the difference being more marked in the second pseudo-Brillouin zone. This suggests that in our polycrystal an additional broadening contribution is present, due to an enhanced phonons scattering from grain boundaries, as well as from the existence of contributions from the minor solid phases. The phonon broadening in the composite is indistinguishable from the amorphous case within error bars in the whole explored q-range.

3.4.2. Transverse modes

We focus first on the first pseudo-Brillouin zone. The existence of a second inelastic excitation here has been already reported in a number of disordered systems, and ascribed to pseudo-transverse modes visible in the longitudinal density fluctuations - as measured in an inelastic x-ray scattering experiment - due to their non-pure polarization (see Ref. [57] and references therein). In this first zone, we observe also for the transverse mode a positive dispersion of the glass speed of sound, much stronger than in the longitudinal case, in agreement with recent calculations [56].

Differently from the longitudinal case, composite and polycrystal display for $q \leq 10$ nm^{-1} a higher transverse speed of sound with respect to the glass, resulting in a macroscopic shear modulus about 12% higher. Many literature studies report on the increase of macroscopic elastic moduli in metallic glasses upon crystallization, showing that the main effect is on the shear modulus. However, the strength of such increase strongly depends on the thermal protocol and final grain size in the crystallized alloy [58, 59, 60].

Here we provide for the first time a direct information on the shear modulus hardening at different lengthscales, going from macroscopic ($q \to 0$) to the atomic scale ($q \approx q_0$). Surprisingly, such hardening is observed only on a macroscopic scale, while at microscopic distances ($q \geq 10$ nm^{-1}, corresponding to $r \leq 6\mathring{A}$) the three systems elastic moduli are indistinguishable from each other. This result is in agreement with the findings of recent structural

investigations in metallic glasses and composites under uniaxial compression, exploiting novel analysis methods to access the strain spatial distribution, and thus the local elastic moduli [61, 62].

Concerning the phonons broadening, no difference is detectable within the experimental uncertainty, which is rather large due to the difficulty of fitting the low energy modes because of a high elastic signal.

We focuse now on the second pseudo-Brillouin zone. We report in Fig. 7 the transverse acoustic dispersion, for a better visualization of the transverse dynamics. The appearance of two transverse-like excitations for the crystalline and the composite samples is quite surprising.

This could be understood in terms of a strong elastic anisotropy of the major crystalline phase, mostly affecting the transverse dynamics, where the orientational average gives then raise to two major contributions, as illustrated in the case of the α-crystobalite polimorph of SiO_2 in Ref. [53]. In order to confirm this interpretation DFT ab-initio calculations of the lattice dynamics of the crystalline phase would be needed, however this remains beyond the scope of the present work.

From Fig. 7 it can be noticed that the glass transverse mode lies between the two transverse modes of the polycrystal, indicating that the elastic anisotropy is washed out by the overall disorder. Still, some residual elastic anisotropy remains, as we can deduce from the phonons width looking to the panel b of Fig. 6. Here, for the polycrystal and the composite, we report the single mode width only in the first zone, while in the second zone, where two modes are present, we have chosen to report the sum of their widths. It can be seen that such sum corresponds roughly to the width of the transverse phonon in the glass. This means that the amorphous phonon, via its width, spans the whole branches distribution of the inelastically anisotropic polycrystal, thus keeping such anisotropy, meaning that the same anisotropic local order is present in the amorphous.

3.5. Total thermal conductivity

Electric and phonons measurements allow us to calculate the electronic and phonon contributions to the thermal conductivity. We first focus on the metallic glass, where, using the Wiedemann-Franz law, we can calculate an electronic contribution of $k_{el} = 4.20 \pm 0.04$ W K^{-1}m^{-1}, i.e. ≈84% of the total thermal conductivity, confirming that this is the dominant heat transport channel, as observed in other metallic glasses [43, 21, 22].

For estimating the phonon contribution, we need first of all to assess the propagative character of the measured modes. For the longitudinal modes, we find that in the whole explored energy range it is $\Gamma < \omega/2\pi$, thus the Ioffe-Regel limit is not reached and longitudinal phonons keep a propagative character over the whole first pseudo-Brillouin zone. As for transverse modes, the opposite is true, the Ioffe-Regel limit being at $q = 7$ nm^{-1}. Nevertheless, we decide to use Eq. 2 to get a first rough estimation of the phonons thermal conductivity, considering that the transverse phonons width remains close to such limit, bypassing it only by 30% at the highest energy point.

We calculate the integral of Eq. 2, using all experimental data measured in the first pseudo-Brillouin zone. In order to do so, we first fit the experimental acoustic dispersions to a sinusoidal behavior, $\omega_L(q) = 24.3(2)sin(0.131(2)q)$ and $\omega_T(q) = 19.2(4)sin(0.114(2)q)$, which allows us to get an analytical expression for the energy dependence of the phonon sound velocities and then estimate the longitudinal and transverse densities of states and the specific heat [63].

We then fit the phonon damping to a quadratic energy dependence for the transverse mode, $\Gamma_T(\omega) = 0.023\omega^2$, while a multi-regime dependence can be observed for the longitudinal broadening. Indeed, data lying below 12 meV escape from a quadratic fit and point more to an ω^4 dependence, consistent to what observed in many glasses at energies close to the Boson Peak [52, 64, 65, 66], which in similar metallic glasses lies in the 5-10 meV range, and in the parent vitreloy MG, Vit4, is at 5 meV [67]. In our energy range, we thus model the longitudinal broadening as $\Gamma_L(\omega) = 0.00008\omega^4$ up to 12 meV, $\Gamma_L(\omega) = 0.013\omega^2$ for $12 \leq \omega \leq 20$ meV and $\Gamma_L(\omega) = 5.2$ meV for $\omega > 20$ meV.

If we limit the integral of Eq. 2 to the experimentally investigated energy range [5–25] meV, a phonon thermal conductivity contribution of only 0.7 W $K^{-1}m^{-1}$ is found. In order to estimate the total contribution, we need to extend the integral down to zero energy, thus making a strong hypothesis on the phonon broadening below our experimental energy range. The ω^4 dependence is known to be limited to a narrow energy range around the Boson Peak, we thus assume that our lowest energy point marks also the lower limit of such behavior, and we recover the ω^2 law for lower energies. With this approximation, a total phonons contribution of 0.95 W $K^{-1}m^{-1}$ is calculated, corresponding to ≈19% of the macroscopic thermal conductivity.

It is first of all important to remind the strong approximations behind this value: 1) we haven't modeled the positive dispersion in the speed of sound, thus slightly overestimating the macroscopic speed of sound, but also neglecting its effects on the calculated density of states [52]; 2) we have under-looked the very complex energy dependence of phonons lifetime in a glass, with our simplistic modeling of the longitudinal and transverse broadening, especially for this latter, having used a single quadratic dependence over all energies; 3) we have assumed transverse phonons as propagative over the whole energy range, while our experimental data lie above the Ioffe-Regel limit. Despite such approximations, the calculated value is well consistent with our calculated electronic contribution and the measured total thermal conductivity, confirming once again that the electronic contribution dominates thermal transport in this glass.

Looking now to the effects of partial and full nanocrystallization on the total thermal conductivity, from the relative weight of electronic and phonon contributions, it is clear that any change related to this latter will be almost negligible. We can quantify it, knowing that the relevant effect of crystallization is only an increase of the transverse speed of sound of ≈6% in the first pseudo-Brillouin zone, while phonons lifetime is basically unaffected. Such change enters Eq. 2 through the phonon velocity and density of states, resulting in an increase of the phonon thermal conductivity of ≈7%, which leads to a phonon-related change

in the total thermal conductivity of less than 2%.

The effect is much more important on the electronic contribution, where the linear decrease of the resistivity results in a linear increase of the electron-related total thermal conductivity of about 18%. Such change, though substantial, is smaller than the experimental uncertainty on our measured values of thermal conductivity, which explains why we could not detect it. Electric measurements are therefore a reliable tool for investigating the effect of nanocrystalline inclusions in metallic glasses on their thermal transport properties, thanks to the higher precision available on electronic measurements with respect to thermal measurements.

4. Conclusion

In this work we have presented a combined macroscopic/microscopic investigation for understanding how thermal transport is modified in presence of nanocrystalline inclusions in a metallic glass. By means of electric resistivity measurements and inelastic x ray scattering measurements, we have been able to disentangle the effects of a partial nanocrystallization onto the two different contributions to heat transport, the electronic and the vibrational one.

No enhanced electrons or phonons scattering from the interfaces is observed in the range of crystalline fractions and grain sizes here investigated. This is in contrast to what reported in Ref. [[33]] on the electric transport of a MG in the early stages of crystallization. As the smallest crystalline fraction here investigated was x=5%, with a grain size of about 4 nm, we can speculate that interface scattering plays a major role only for even smaller grain sizes and crystalline fractions, at the very beginning of the crystallization. A steady increase of the electronic contribution is instead observed, which accounts almost for the whole change in the total thermal conductivity.

Concerning the vibrational contribution, we find that a partial nanocrystallization of about 30% leads to an increase of the transverse acoustic speed of sound in the first Brillouin zone, which in turn reflects into an increase of the total

thermal conductivity, but of only 2%, remaining a negligible contribution in this metallic system.

The fully crystalline sample on the other hand exhibits a high electric resistivity and important phonon broadening, which result in electric and thermal transport properties very close to the parent MG, likely due to the dominant effect of grain booundaries scattering as well as scattering from a kind of disorder on the mesoscopic scale, given by the mixture of three solid phases.

It is worth underlying that in the composite, the crystal-like behavior appears to dominate phonons properties already for a crystalline fraction of 30% on all explored lengths scales, down to the nearest neighbors distance ($q \approx q_0$). The situation is different for the electronic properties, where the composite is always described by an effective medium theory, where crystalline and amorphous contributions are weighted with their volume fraction, and the crystalline part starts to dominate only for volume fractions larger than 60%, as indicated by the change of sign of the TCR. A low crystalline fraction is therefore enough for inducing an important change in the elastic moduli, while keeping an electric resistivity typical of an amorphous alloy.

The results presented here indicate thus that partially nanocrystallized metallic glasses with crystalline fractions lower than 50% are promising composites for a wide panel of applications, thanks to a higher ductility, larger elastic moduli and almost no modification of thermal and electric transport properties, which assess them as improved materials with respect to both amorphous and crystalline alloys.

Aknowledgments

Financial support by the Rhone-Alpes region through the ARC Energie funding program is aknowledged. The authors thank the staff of ID28 at the ESRF for experimental support, J. Faria for help during the IXS experiment, R. Vera of the x ray diffraction center H. Lonchambon for technical help and M. De Boissieu for fruitful discussion.

References

[1] A. Inoue, Stabilization of metallic supercooled liquid and bulk amorphous alloys, Acta Mat. 48 (2000) 279–306.

[2] C. A. Schuh, T. C. Hufnagel, U. Ramamurty, Mechanical behavior of amorphous alloys, Acta Mat. 55 (2007) 40674109.

[3] W. Wang, C. Dong, C. Shek, Bulk metallic glasses, Materials Science and Engineering R 44 (2004) 4589.

[4] M. Ashby, A. Greer, Metallic glasses as structural materials, Scripta Materialia 54 (2006) 321326.

[5] W. H. Wang, D. W. He, D. Q. Zhao, Y. S. Yao, M. He, Nanocrystallization of zrticunibec bulk metallic glass under high pressure, Appl. Phys. Lett. 75 (1999) 2770.

[6] J.-J. Kim, Y. Choi, S. Suresh, A. S. Argon, Nanocrystallization during nanoindentation of a bulk amorphous metal alloy at room temperature, Science 295 (2002) 654–657.

[7] C. Fan, A. Inoue, Improvement of mechanical properties by precipitation of nanoscale compound particles in zr-cu-pd-al amorphous alloys, Materials transactions 38 (1997) 1040–1046.

[8] K. Hajlaoui, A. Yavari, A. LeMoulec, W. Botta, F. Vaughan, J. Das, A. Greer, A. . Kvick, Plasticity induced by nanoparticle dispersions in bulk metallic glasses, Journal of Non-Cryst. Solids 353 (2007) 327–331.

[9] S.-W. Lee, M.-Y. Huh, E. Fleury, J.-C. Lee, Crystallization-induced plasticity of cuzr containing bulk amorphous alloys, Acta Materialia 54 (2006) 349355.

[10] H. Chen, Y. He, G. Shiflet, S. Poon, Mechanical properties of partially crystallized aluminum based metallic glasses, Scripta Matallurgica et Materialia 25 (1991) 1421.

[11] Y. H. Kim, A. Inoue, T. Masumoto, Ultrahigh tensile strengths of al88y2ni9m1 (m=mn or fe) amorphous alloys containing finely dispersed fcc-al particles, Mater. Trans. JIM 31 (1990) 747.

[12] T. Brink, M. Peterlechner, H. Rsner, K. Albe, G. Wilde, Influence of crystalline nanoprecipitates on shear-band propagation in cu-zr-based metallic glasses, Phys. Rev. B 5 (2016) 054005.

[13] Y. C. Kim, J. H. Na, J. M. Park, D. H. Kim, J. K. Lee, W. T. Kim, Role of nanometer-scale quasicrystals in improving the mechanical behavior of ti-based bulk metallic glasses, Appl. Phys. Lett. 83 (2003) 3093.

[14] M. Heilmaier, Deformation behavior of zr-based metaliic glasses, Journal of Materials Processing Technology 117 (2001) 374.

[15] T. Kulik, Nanocrystallization of metallic glasses, Journal of Non-Cryst. Solids 287 (2001) 145.

[16] J. Wang, R. Li, N. Hua, L. Huang, T. Zhang, Ternary fepc bulk metallic glass with good soft-magnetic and mechanical properties, Scripta Materialia 65 (2011) 536.

[17] Z. Jiao, H. Li, J. Gao, Y. Wu, Z. Lu, Effects of alloying elements on glass formation, mechanical and soft-magnetic properties of fe-based metallic glasses, Intermetallics 19 (2011) 1502.

[18] D. C. Hofmann, J.-Y. Suh, A. Wiest, G. Duan, M.-L. Lind, M. D. Demetriou, W. Johnson, Designing metallic glass matrix composites with high toughness and tensile ductility, Nature Letters 451 (2008) 1085.

[19] D. C. Hofmann, J.-Y. Suh, A. Wiest, M.-L. Lind, M. D. Demetriou, W. L. Johnson, Development of tough, low-density titanium-based bulk metallic glass matrix composites with tensile ductility, PNAS 105 (2008) 2013620140.

[20] J. W. Qiao, S. Wang, Y. Zhang, P. K. Liaw, G. L. Chen, Large plasticity and tensile necking of zr-based bulk-metallic-glass-matrix composites synthesized by the bridgman solidification, Appl. Phys. Lett. 94 (2009) 151905.

[21] U. Harms, T. Shen, R. Schwarz, Thermal conductivity of pd40ni40-xcuxp20 metallic glasses, Scripta Materialia 47 (2002) 411–414.

[22] R. Y. Umetsu, R. Tu, T. Goto, Thermal and electrical transport properties of zr-based bulk metallic glassy alloys with high glass-forming ability, Materials Transactions 53 (2012) 1721–1725.

[23] H. Y. Bai, C. Z. Tong, P. Zheng, Electrical resistivity in zr48nb8cu12fe8be24 glassy and crystallized alloys, Journal of Applied Physics 95 (2004) 1269.

[24] Y. K. Kuo, K. M. Sivakumar, C. A. Su, C. N. Ku, S. T. Lin, A. B. Kaiser, J. B. Qiang, Q. Wang, C. Dong, Measurement of low-temperature transport properties of cu-based cu-zr-ti bulk metallic glass, Phys. Rev. B 74 (2006) 014208.

[25] J. Z. Jiang, W. Roseker, C. S. Jacobsen, G. F. Goya, Low-temperature electrical resistivity of as-cast glassy, relaxed, and crystallized pd40cu30ni10p20 alloys, J. Phys. Cond. Matter 15 (2003) 8713–8718.

[26] H. Gleiter, Nanocrystalline materials, Progress in Materials Science 33 (1989) 223–315.

[27] U. Mizutani, Electron transport properties of non-magnetic metallic glasses, Materials Science and Engineering 99 (1988) 165–173.

[28] U. Mizutani, M. Tanaka, H. Sato, Studies of negative tcr and electronic structure of nonmagnetic metallic glasses based on y and la., Journal of Physics F: Metal Physics 17 (1987) 131–141.

[29] O. Haruyama, T. Miyazawa, J. Saida, A. Inoue, Change in electrical resistivity due to icosahedral phase precipitation in zr 70 pd 20 ni 10 and zr 65 al 7.5 cu 7.5 ni 10 ag 10 glasses, Applied Physics Letters 79 (2001) 758.

[30] S. J. Chung, K. T. Hong, M.-R. Ok, J.-K. Yoon, G.-H. Kim, Y. S. Ji, B. S. Seong, K. S. Lee, Analysis of the crystallization of zr41ti14cu12.5ni10be22.5 bulk metallic glass using electrical resistivity measurement, Scripta Materialia 53 (2005) 223228.

[31] Y. S. Ji, S. J. Chung, M.-R. Ok, K. T. Hongb, J.-Y. Suh, J. W. Byeon, J.-K. Yoon, K. H. Lee, K. S. Lee, Analysis on the phase transition behavior of cu base bulk metallic glass by electrical resistivity measurement, Materials Science and Engineering A 449-451 (2007) 521.

[32] A. J. Kailathy, K. Dutta, T. C. Alex, A. Mitra, Crystallization study of cu56zr7ti37 metallic glass by electrical resistivity measurement, J. Mater. Sci. Technol 27 (2011) 275–279.

[33] B. Liu, N. Zuo, F. Ye, Abnormal change of electrical resistivity in the cu46zr46al8 bulk metallic glass during crystallization, Materials Letters 171 (2016) 285–288.

[34] E. G. Fu, J. Carter, M. Martin, G. Xie, X. Zhang, Y. Wang, R. Littleton, S. McDeavitt, L. Shao, Ar-ion-milling-induced structural changes of cu50zr45ti5 metallic glass, Nuclear Instruments and Methods in Physics Research B 268 (2010) 545.

[35] D. Nagahama, T. Ohkubo, T. Mukai, K. Hono, Characterization of nanocrystal dispersed cu60zr30ti10 metallic glass, Materials Transactions 46 (2005) 1264.

[36] C. Williams, H. Wickramasinghe, Scanning thermal profiler, Applied Physics Letters 49 (1986) 1587.

[37] B. Cretin, S. Gomes, N. Trannoy, P. Vairac, Scanning thermal microscopy, Microscale and nanoscale heat transfer, volume 107, 181-238 ed., Springer, 2007.

[38] C. Masciovecchio, U. Bergmann, M. Krisch, G. Ruocco, F. Sette, R. Verbeni, Nucl. Instrum. Methods Phys. Res. B 111 (1996) 181.

[39] C. Masciovecchio, U. Bergmann, M. Krisch, G. Ruocco, F. Sette, R. Verbeni, Nucl. Instrum. Methods Phys. Res. B 117 (1996) 339.

[40] R. Verbeni, F.Sette, M. Krisch, U. Bergmann, B. Gorges, C. Halcoussis, K. Martel, C. Masciovecchio, J. F. Ribois, G. Ruocco, H. Sinn, J. Synchrotron Radiat. 3 (1996) 62.

[41] S. Gravier, P. Donnadieu, S. Lay, B. Doisneau, F. Bley, L. Salvo, J. Blandin, Evaluation of the crystal volume fraction in a partially nanocrystallized bulk metallic glass, Journal of Alloys and Compounds 504S (2010) S226–S229.

[42] J. Langford, A. Wilson, Scherrer after sixty years: A survey and some new results in the determination of crystallite size, J. Appl. Cryst. 11 (1978) 102–113.

[43] M. Yamasaki, S. Kagao, Y. Kawamura, K. Yoshimura, Thermal diffusivity and conductivity of supercooled liquid in zr41ti14cu12ni10be23 metallic glass, Appl. Phys. Lett. 84 (2004) 4653.

[44] Z. Zhou, C. Uher, D. Xu, W. L. Johnson, W. Gannon, M. C. Aronson, On the existence of einstein oscillators and thermal conductivity in bulk metallic glass, Appl. Phys. Lett. 89 (2006) 031924.

[45] P. J. Cote, L. V. Meisel, Electrical Transport in Glassy Metals, volume 46 of *Topics in Applied Physics*, Springer, 1981.

[46] J.-B. Vaney, A. Piarristeguy, V. Ohorodniichuck, O. Ferry, A. Pradel, E. Alleno, J. Monnier, E. B. Lopes, A. P. Goncalves, G. Delaizir, C. Candolfi,

A. Dauscher, B. Lenoir, Effective medium theory based modeling of the thermoelectric properties of composites: Comparison between predictions and experiments in the glass-crystal composite system si10as15, Journal of Materials Chemistry C 3 (2015) 11090–11098.

[47] H. Euchner, S. Pailhès, L. T. K. Nguyen, W. Assmus, F. Ritter, A. Haghighirad, Y. Grin, S. Paschen, M. de Boissieu, Phononic filter effect of rattling phonons in the thermoelectric clathrate ba8ge40+xni6?x., Phys. Rev. B 86 (2012) 224303.

[48] P.-F. Lory, S. Pailhès, V. M. Giordano, H. Euchner, H. D. Nguyen, R. Ramlau, H. Borrmann, M. Schmidt, M. Baitinger, M. Ikeda, P. Tomes, M. Mihalkovic, C. Allio, M. R. Johnson, H. Schober, Y. Sidis, F. Bourdarot, L. P. Regnault, J. Ollivier, S. Paschen, Y. Grin, M. de Boissieu, Long-living heat carriers in a crystalline poor thermal conductor, Nat. Comm. (under review) (2017).

[49] B. Allen, J. L. Feldman, Phys. Rev. B 48 (1993) 12581.

[50] G. Baldi, V. M. Giordano, G. Monaco, F. Sette, E. Fabiani, A. FOntana, G. Ruocco, Thermal conductivity and terahertz vibrational dynamics of vitreous silica, Phys. Rev. B 77 (2008) 214309.

[51] V. M. Giordano, G. Monaco, Fingerprints of order and disorder on the high-frequency dynamics of liquids, PNAS 107 (2010) 21985.

[52] G. Monaco, V. M. Giordano, Breakdown of the debye approximation for the acoustic modes with nanometric wavelengths in glasses, PNAS 106 (2009) 3659.

[53] A. Bosak, M. Krisch, I. Fischer, S. Huotari, G. Monaco, Inelastic x-ray scattering from polycrystalline materials at low momentum transfer., Phys. Rev. B Condens. Matter Mater. Phys. 75 (2007) 064106.

[54] T. Ichitsubo, S. Hosokawa, K. Matsuda, E. Matsubara, N. Nishiyama, S. Tsutsui, A. Q. R. Baron, Nanoscale elastic inhomogeneity of a pd-based

metallic glass: Sound velocity from ultrasonic and inelastic x-ray scattering experiments, Phys. Rev. B 76 (2007) 140201(R).

[55] T. Ichitsubo, H. Kato, E. Matsubara, S. Biwa, S. Hosokawa, K. Matsuda, H. Uchiyama, A. Baron, Static heterogeneity in metallic glasses and its correlation to physical properties, J. Non-Cryst. Sol. 357 (2011) 494–500.

[56] D. Crespo, P. Bruna, A. Valles, E. Pineda, Phonon dispersion relation of metallic glasses, Phys. Rev. B 94 (2016) 144205.

[57] V. V. Brazhkin, K. Trachenko, Collective excitations and thermodynamics of disordered state: New insights into an old problem, J. Phys. Chem. B 118 (2014) 11417–11427.

[58] M. Idriss, F. Clari, Y. Yokoyama, F. Tessier, T. Rouxel, Evolution of the elastic modulus of zrcual bmgs during annealing treatment and crystallization: Role of zr/cu ratio, J. Non-Cryst. Sol. 421 (2015) 35–40.

[59] G. E. Abrosimova, N. P. Kobelev, E. L. Kolyvanov, V. A. Khonik, The influence of heat treatment on the ultrasonic velocity and elastic moduli of a zrcunialti bulk metallic glass, Physics of the Solid State 46 (2004) 1859–1862.

[60] G. E. Abrosimova, N. P. Kobelev, E. L. Kolyvanov, V. A. Khonik., V. M. Levin, Y. S. Petronyuk, Effect of heat treatment on the elastic characteristics of a bulk amorphous zrcunialti alloy, Physics of the Solid State 48 (2006) 2091–2094.

[61] H. F. Poulsen, J. A. Wert, J. Neuefeind, V. Honkimaki, M. Daymond, Measuring strain distributions in amorphous materials, Nat. Mat. 4 (2005) 33.

[62] T. C. Hufnagel, R. T. Ott, Structural aspects of elastic deformation of a metallic glass, Phys. Rev. B 73 (2006) 064204.

[63] C. Kittel, Introduction to Solid State Physics, 1996.

[64] G. Baldi, V. M. Giordano, G. Monaco, B. Ruta, Sound attenuation at terahertz frequencies and the boson peak of vitreous silica, Phys. Rev. Lett. 104 (2010) 195501.

[65] B. Rufflé, Phys. Rev. Lett. 90 (2003) 095502.

[66] B. Rufflé, Phys. Rev. Lett. 96 (2006) 045502.

[67] Y. Li, P. Yu, H. Y. Bai, Study on the boson peak in bulk metallic glasses, J. Appl. Phys. 104 (2008) 013520.

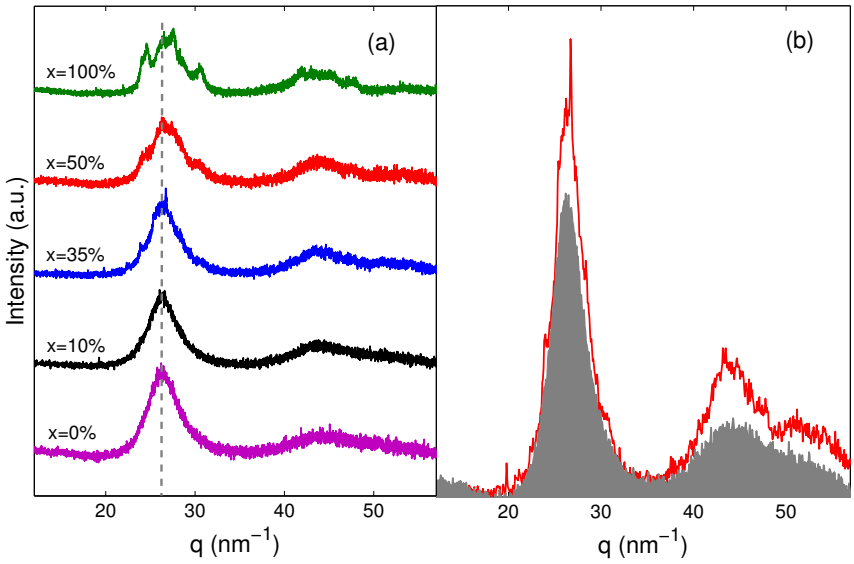

Figure 1: *(Color online)***Structural characterization** (a) X-ray diffraction (XRD) patterns measured at room temperature on samples with different crystalline fraction x (%). The intensity is reported as a function of the scattering wavevector q after background subtraction. The vertical dashed line marks position of the FSDP q_0.(b) Estimation of the crystalline fraction from XRD patterns: the amorphous pattern (shadowed grey) measured prior to crystallization is scaled until it matches the remaining amorphous contribution in the composite pattern (red). In the reported case, it results x=35 $\pm$ 2 %.

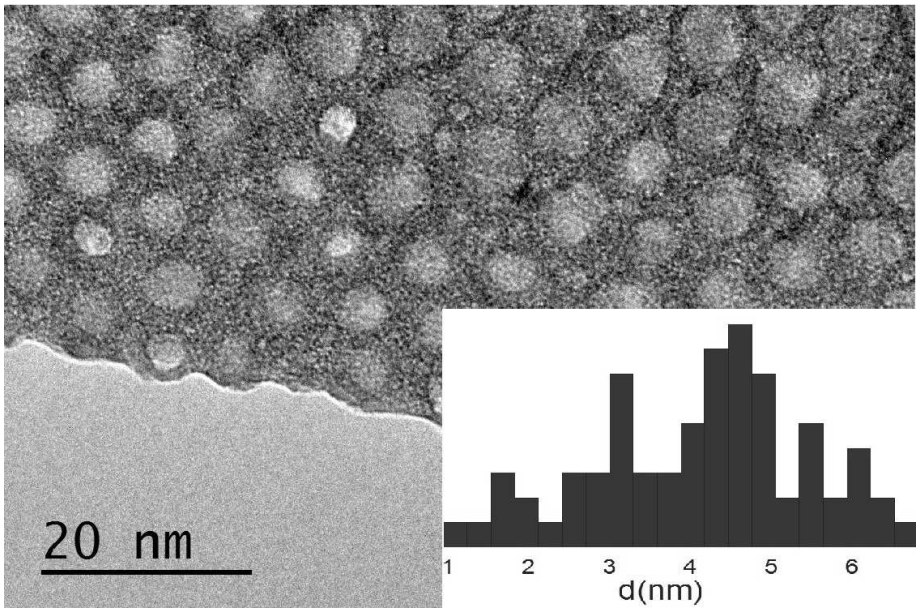

Figure 2: *(Color online)***TEM image of a composite** Dark field TEM image collected in a composite with crystalline fraction x=50%; from the analysis of the image the crystalline diameters distribution is obtained and shown in the inset, with a crystalline mean diameter $d \approx 4 \pm 2$ nm.

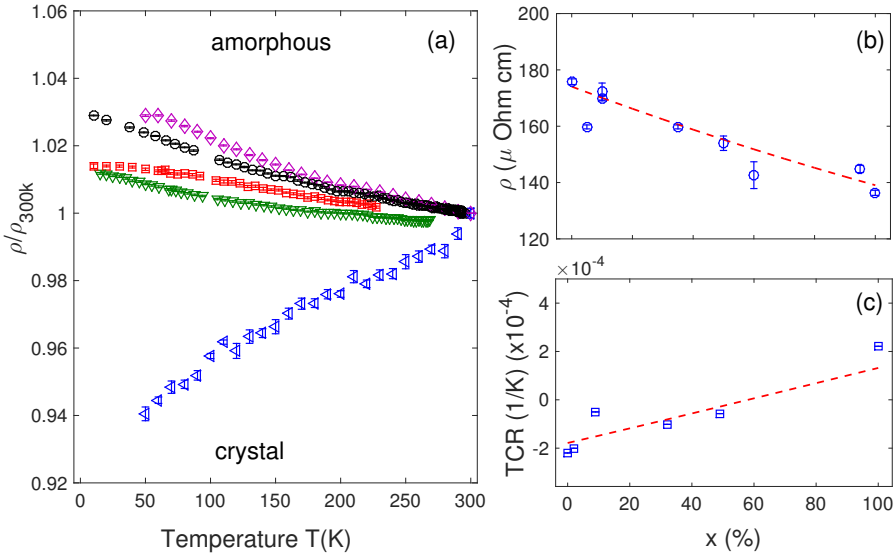

Figure 3: *(Color online)***Electrical Resistivity** (a) Temperature dependence of electrical resistivity renormalized at the room temperature value, for the amorphous (violet), crystalline (blue) and some representative composite samples with x=35% (black), x=10% (red), x=60% (green). (b) Room temperature electrical resistivity as a function of crystalline fraction. The prediction of the effective medium theory is reported as a dashed line. (c) Evolution of the TCR (see text) as a function of crystalline fraction. The prediction of the effective medium theory is reported as a dashed line.

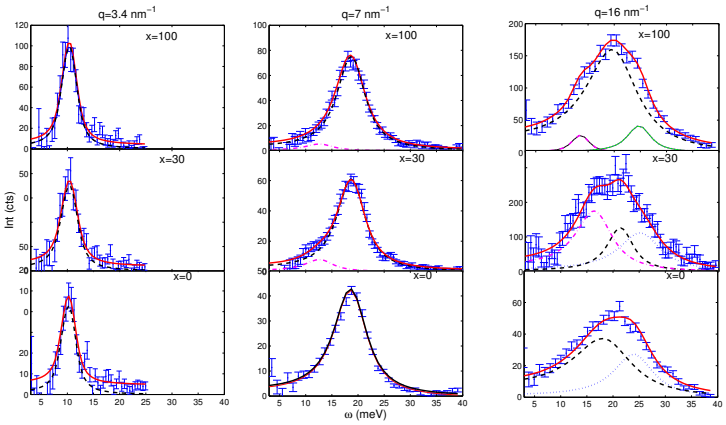

Figure 4: *(Color online)* **Inelastix X ray Scattering Results** IXS spectra collected at three different momentum transfer q in the fully amorphous (x=0, bottom line), partially crystalline (x=30, middle line) and fully crystalline (x=100, top line) samples, after elastic line subtraction. The first 2 columns correspond to q values in the first pseudo-Brillouin zone, the left column to a q lying in the second pseudo-Brillouin zone. The red line corresponds to the fit with a multi-modes model, whose components are also reported in black, magenta and blue. Details are in the text.

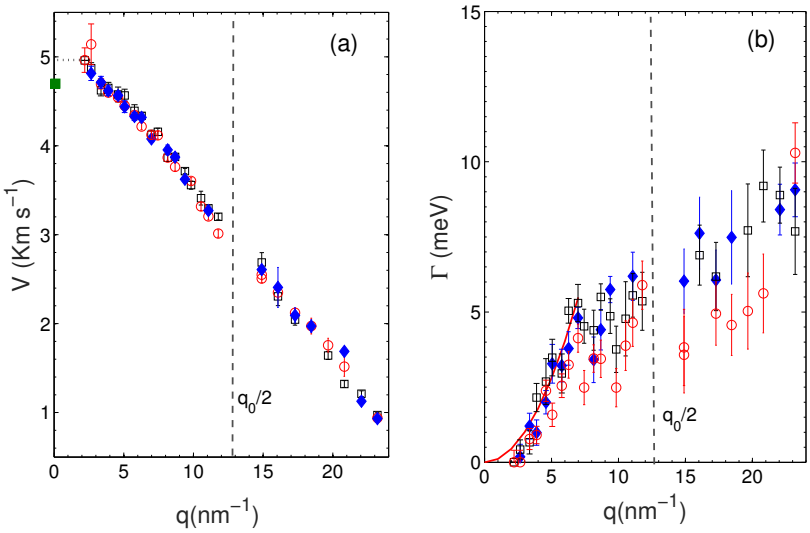

Figure 5: *(Color online)***Longitudinal velocity and attenuation** Longitudinal sound velocity (a) and phonon broadening (b) as a function of wave vector q: for the amorphous sample (black squares), the fully crystalline sample (red circles) and a composite with x=30 % (blue full diamonds). A vertical dashed gray line marks the pseudo-Brillouin zone border. (a): The macroscopic longitudinal sound velocity for the amorphous sample measured by ultrasound technique is also reported as a green square. The low q limit of the amorphous longitudinal speed of sound is marked with a horizontal dotted line. (b): the red solid line corresponds to the fit of amorphous data to a q^2 behavior.

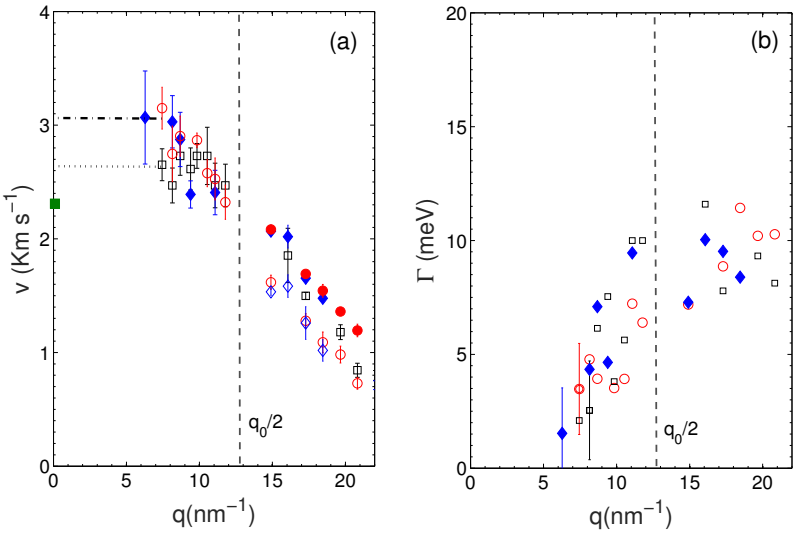

Figure 6: *(Color online)* **Transverse velocity and attenuation** Transverse sound velocity (a) and phonon broadening (b) as a function of wavevector q for the amorphous (black squares), the fully crystalline sample (red circles) and a composite with x=30% (blue full diamonds). A vertical gray dashed line marks the pseudo-Brillouin zone border. (a): In the second zone, full and empty red circles and blue diamonds correspond to the two transverse modes of the fully and partially crystalline samples respectively. The macroscopic transverse sound velocity of the amorphous sample measured by ultrasound technique is also reported as a green square. Horizontal lines mark the low q limit for the transverse speed of sound in the glass (dotted line) and the polycrystal and composite (dot-dashed line) (b): A representative error bar on the broadening is reported only for one data point per dataset for better visual clarity. Data for the partially and fully crystalline samples in the second zone correspond to the sum of the two transverse modes width in this zone, to be compared with the width of the single transverse mode in the glass.

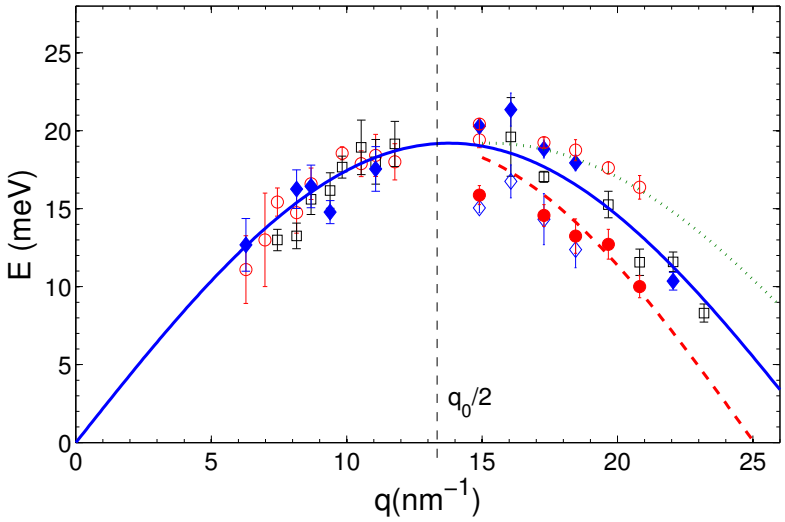

Figure 7: *(Color online)***Transverse acoustic dispersion** Transverse acoustic dispersion for the glass (black square), the polycrystal (full and empty red circles) and the composite (full and empty blue diamonds). The solid line is a sinusoidal fit of the glass data, dotted and dashed line describe the two transverse branches of the polycrystalline and composite samples in the second zone.